

## COMPARISON OF THE DISCRETE SINGULAR CONVOLUTION AND THREE OTHER NUMERICAL SCHEMES FOR SOLVING FISHER'S EQUATION\*

SHAN ZHAO<sup>†</sup> AND G. W. WEI<sup>‡</sup>

**Abstract.** In this paper, a discrete singular convolution (DSC) algorithm is introduced to solve Fisher's equation, to which obtaining an accurate and reliable traveling wave solution is a challenging numerical problem. Two novel numerical treatments, a moving frame scheme and a new asymptotic scheme, are designed to overcome the subtle difficulties involved in the numerical solution of Fisher's equation. The moving frame scheme is proposed to provide accurate and efficient spatial resolution of the problem. The new asymptotic scheme is introduced to facilitate the correct prediction of the wave speed after long-time integrations. The resulting DSC algorithm is able to correctly predict long-time traveling wave behavior. The performance of the present algorithm is demonstrated through extensive numerical experiments as well as through a comparison with three other standard approaches, i.e., methods of the Fourier pseudospectral, the accurate spatial derivatives, and the Crank–Nicolson schemes. The spatial and temporal accuracies of all four methods are analyzed and numerically verified.

**Key words.** Fisher's equation, discrete singular convolution, Fourier pseudospectral method

**AMS subject classifications.** 35K15, 65M06, 65M70, 65M99

**DOI.** 10.1137/S1064827501390972

**1. Introduction.** Fisher [3] introduced a one-dimensional nonlinear parabolic partial differential equation (PDE) to describe the kinetic advancing rate of an advantageous gene,

$$(1.1) \quad \frac{\partial u}{\partial t} = \mu \frac{\partial^2 u}{\partial x^2} + \rho u(1 - u), \quad x \in (-\infty, \infty), \quad t > 0,$$

where the positive quantities  $\mu$  and  $\rho$  are the diffusion coefficient and the reaction factor, respectively. Fisher's equation represents the evolution of the population due to the two competing physical processes, diffusion and nonlinear local multiplication. Equation (1.1) also describes a prototype model for a spreading flame [9] and a model equation for the finite domain evolution of neutron population in a nuclear reactor [1].

It is convenient to nondimensionalize (1.1) by means of the transformation  $t := \rho t$ ,  $x := (\rho/\mu)^{1/2}x$  so that Fisher's equation returns a simpler form,

$$(1.2) \quad \frac{\partial u}{\partial t} = \frac{\partial^2 u}{\partial x^2} + u(1 - u).$$

With the assumption that the saturation level is unity, the different initial and boundary conditions (BCs) for Fisher's equation read

---

\*Received by the editors October 15, 2001; accepted for publication (in revised form) March 17, 2003; published electronically September 9, 2003. This work was supported in part by the National University of Singapore and Michigan State University.

<http://www.siam.org/journals/sisc/25-1/39097.html>

<sup>†</sup>Department of Computational Science, National University of Singapore, Singapore 117543 (asan@cz3.nus.edu.sg).

<sup>‡</sup>Department of Mathematics, Michigan State University, East Lansing, MI 48824 (wei@math.msu.edu).

$$(1.3) \quad u(x, 0) = u_0(x) \in [0, 1], \quad x \in (-\infty, \infty),$$

$$(1.4) \quad \lim_{x \rightarrow -\infty} u(x, t) = 1, \quad \lim_{x \rightarrow \infty} u(x, t) = 0,$$

$$(1.5) \quad \lim_{x \rightarrow \pm\infty} u(x, t) = 0,$$

with the  $x$  derivative tending to zero as  $x \rightarrow \pm\infty$ . In the literature, conditions (1.3) and (1.4) together are commonly referred to as nonlocal conditions, while conditions (1.3) and (1.5) together are usually referred to as local conditions.

The properties of Fisher's equation have been studied theoretically by many authors, including Fisher [3], Kolmogorov, Petrovshy, and Piscounoff [9], Canosa [1], Larson [10], Hagan [7], etc. For the nonlocal conditions (1.3) and (1.4), it is proved in [9] that for every value of  $c \geq 2$ , there exists a traveling wave solution to (1.2) with a wave speed  $c$ . No such solution exists if  $c < 2$ . The traveling wave solution can be expressed in the form  $u(x, t) = V(x - ct)$  for a certain function  $V$  of the single scalar independent variable  $z = x - ct$ . Such a solution is bounded as  $u_0(x)$  in (1.3), i.e.,  $V(z) \in [0, 1]$  for any  $z \in \mathbb{R}$ . For a given initial datum, the wave speed of the steady state solution of Fisher's equation is unique. Larson [10] and Hagan [7] discovered an interesting phenomenon in which the steady state wave speed depends crucially on the behavior of the initial datum at infinity. In particular, if  $u_0(x) \sim e^{-\beta x}$  as  $x \rightarrow \infty$ , then, as  $t \rightarrow \infty$ , the solution evolves to a traveling wave of speed  $c(\beta)$  given by

$$(1.6) \quad c(\beta) = \begin{cases} \beta + \frac{1}{\beta}, & \beta \leq 1, \\ 2, & \beta \geq 1. \end{cases}$$

The traveling wave solution of Fisher's equation has also been studied numerically by many researchers because the accurate and reliable numerical representation of the traveling wave solution to Fisher's equation is an interesting and challenging numerical problem. Numerous computational approaches have been applied to Fisher's equation in the literature, including the method of accurate space derivatives (ASD) [6], finite differences [8, 13, 14], finite elements [20, 2, 18], as well as many others [15, 22, 12, 11, 16, 17].

In any numerical study of Fisher's equation, the infinite physical domain has to be truncated into a finite computational domain  $[x_L, x_R]$ , with approximate BCs imposed at  $x = x_L$  and  $x = x_R$ . One of the most difficult numerical problems for the solution of Fisher's equation is the sensitivity of a correct numerical solution to the appropriate BCs, especially the one imposed at the right-hand boundary [6, 8, 16]. Theoretical study reveals that it is the initial data at infinity that determine the traveling speed of the steady state wave solution. In numerical studies, the wave speed of the simulated traveling wave is determined by the BC applied on  $x = x_R$  at each step of the time integration. Therefore, incorrect results would be obtained unless certain proper BCs are applied.

The commonly used BCs for Fisher's equation in the literature [6, 15, 2, 17] include  $u(x_L, t) = 1$  and  $u(x_R, t) = 0$  for nonlocal conditions and  $u(x_L, t) = 0$  and  $u(x_R, t) = 0$  for local conditions. By using such BCs, Gazdag and Canosa [6] demonstrated that the superspeed wave (SSW) (the wave with speed  $c > 2$ ) with theoretical speed  $c = 4$  or  $c = 6$  quickly evolves into the minimum speed wave. They also found that the time of evolving from SSW to the minimum speed wave depends crucially on the boundary cutoff point  $x_R$ . Carey and Shen [2] reported similar results by using a different numerical scheme under the same BCs. In some recent work on the numerical solution of Fisher's equation, Li, Petzold, and Ren [11] and Qiu and

Sloan [16] avoided this difficulty by directly using the exact solution values in the Dirichlet BC. However, this treatment is not applicable for general numerical studies. An interesting exception reported in the literature is the BC given by Hagstrom and Keller [8]. In terms of an asymptotic expansion form, their BC explicitly takes into account the initial data in the discarded region  $x > x_R$ . By using it, the traveling wave solutions with superspeed can be accurately represented on a finite domain. However, their BC is relatively complex and an explicit representation of the initial data at infinity is required, which is actually unavailable in general.

Another difficulty of the numerical solution of Fisher's equation is the instability of the traveling wave with respect to a small perturbation at the front of the wave [6, 7, 16]. It has been shown that the traveling wave is stable to a small disturbance of compact support, while it is unstable under a small disturbance of infinite support [6, 7]. Qiu and Sloan further commented that perturbations at the wave front are very significant compared with those at the rear of the wave. In numerical studies, as noted by Carey and Shen [2], a slight negative value in the wave front will develop into a noticeably negative undershoot. Therefore, the stability and reliability of numerical schemes are of crucial importance to the sound simulation of the long-term behavior of the traveling wave solution.

Recently, Li, Petzold, and Ren [11] considered the numerical solution of a scaled Fisher's equation with very strong reaction. Under such strong reaction, the solution evolves into a shock-like wave, which is difficult to resolve by using a uniform coarse grid with a traditional lower-order scheme. The authors of [11] attacked the problem by using a popular moving mesh method able to dynamically generate a suitable nonuniform mesh. However, their results are not satisfactory. More recently, Qiu and Sloan [16] re-examined the problem. They showed that by modifying the monitor function, the moving mesh method can perform well for the strong reaction case.

Most recently, the discrete singular convolution (DSC) algorithm [24] was proposed as a potential numerical approach for solving many computational problems, including Hilbert transform, analytic signal processing, and computational tomography. The mathematical foundations of the algorithm are the theory of distributions and the theory of wavelets [28]. The use of the DSC algorithm was demonstrated by solving problems of quantum eigenvalues [25], linear and nonlinear dynamics [26], incompressible flows [29], and structural analysis [31, 32]. The DSC algorithm was also successfully utilized to facilitate a new synchronization scheme for shock capturing [30]. In [27], the unified feature of the DSC formalism was discussed and there it was demonstrated that computational methods of Galerkin, collocation, global, local, and finite difference types can be derived from a single starting point in the framework of the DSC algorithm.

The objective of the present work is fourfold. First, we explore the use of the DSC algorithm as a unified approach for solving Fisher's equation. Our second objective is to make a comparison of the Fourier pseudospectral (FPS) method [19], the ASD approach [6], the DSC scheme, and the Crank–Nicolson (CN) scheme for solving Fisher's equation. Third, we introduce a moving frame method to resolve the shock-like wave. Finally, we propose a new asymptotic scheme to ensure a correct traveling speed.

This paper is organized as follows. Section 2 is devoted to a brief description of the DSC, CN, FPS, and ASD schemes. Section 3 gives some analyses of four numerical schemes with respect to spatial resolution and time integration. Section 4 presents the application of four numerical schemes to the solution of Fisher's equation.

Only the nontrivial SSW is studied in the present work, since it is numerically very difficult compared with the minimum speed wave. Extensive numerical experiments are carried out to verify the theoretical analyses and to compare the accuracy, stability, flexibility, and efficiency of the four numerical schemes. Both the analytical solution and the steady state wave speed are invoked for a quantitative validation of the present approaches. Conclusions are presented in section 5.

## 2. Numerical methods.

**2.1. Discrete singular convolution.** Singular convolutions are a special class of mathematical transformations which appear in many science and engineering problems such as Hilbert transform, Abel transform, and Radon transform. It is most convenient to discuss the singular convolution in the context of the theory of distributions. Let  $T$  be a distribution and  $\eta(t)$  be an element of the space of test functions. A singular convolution is defined as

$$(2.1) \quad F(t) = (T * \eta)(t) = \int_{-\infty}^{\infty} T(t-x)\eta(x)dx.$$

Here  $T(t-x)$  is a singular kernel. Depending on the form of the kernel  $T$ , the singular convolution is the central issue for a wide range of science and engineering problems.

An important example that is relevant to the present study involves the singular kernels of delta type  $T(x) = \delta^{(n)}(x)$ , ( $n = 0, 1, 2, \dots$ ). Here, kernel  $T(x) = \delta(x)$  is of particular importance for the interpolation. Higher-order kernels,  $T(x) = \delta^{(n)}(x)$ , ( $n = 1, 2, \dots$ ) are essential for numerically solving PDEs and for image processing, noise estimation, etc. However, since these kernels are singular, they cannot be directly digitized in computers. Hence, the singular convolution, (2.1), is of little numerical merit. To avoid the difficulty of using singular expressions directly in computers, we construct sequences of approximations ( $T_\alpha$ ) to the distribution  $T$ ,  $\lim_{\alpha \rightarrow \alpha_0} T_\alpha(x) \rightarrow T(x)$ , where  $\alpha_0$  is a generalized limit. Note that one retains the delta distribution at the limit. Computationally, the Fourier transform of the delta distribution is unity. Hence, it is a *universal reproducing kernel* for numerical computations and an *all pass filter* for image and signal processing. Therefore, the delta distribution can be used as a starting point for the construction of either band-limited reproducing kernels or approximate reproducing kernels. By the Heisenberg uncertainty principle, exact reproducing kernels have bad localization in the time (spatial) domain, whereas approximate reproducing kernels can be localized in both time and frequency representations. Furthermore, with a sufficiently smooth approximation, it is useful to consider a DSC

$$(2.2) \quad F_\alpha(t) = \sum_k T_\alpha(t-x_k)f(x_k),$$

where  $F_\alpha(t)$  is an approximation to  $F(t)$  and  $\{x_k\}$  is an appropriate set of discrete points on which the DSC, (2.2), is well defined. Note that the original test function  $\eta(x)$  has been replaced by  $f(x)$ . The mathematical property or requirement for  $f(x)$  is determined by the approximate kernel  $T_\alpha$ .

The delta distribution or the so-called Dirac delta function ( $\delta$ ) is a generalized function which is integrable inside a particular interval but in itself need not have a value. It is given as a continuous linear functional on the space of test functions  $\mathcal{D}(-\infty, \infty)$ ,  $\langle \delta, \phi \rangle = \delta(\phi) = \int_{-\infty}^{\infty} \delta \phi = \phi(0)$ . A delta sequence kernel,  $\{\delta_\alpha(x)\}$ , is a sequence of kernel functions on  $(-\infty, \infty)$  which are integrable over every compact

domain, and their inner product with every test function  $\phi$  converges to the delta distribution

$$(2.3) \quad \lim_{\alpha \rightarrow \alpha_0} \int_{-\infty}^{\infty} \delta_{\alpha} \phi = \langle \delta, \phi \rangle,$$

where the (real or complex) parameter  $\alpha$  approaches  $\alpha_0$ , which can be either  $\infty$  or a limit value, depending on the situation (such a convention for  $\alpha_0$  is used throughout this paper). If  $\alpha_0$  represents a limit value, the corresponding delta sequence kernel is a fundamental family.

There are many delta sequence kernels arising in the theory of PDEs, Fourier transforms, and signal analysis, with completely different mathematical properties. The delta sequence kernels of Dirichlet type have very distinct mathematical properties and are used in the present work. Let  $\{\delta_{\alpha}\}$  be a sequence of functions on  $(-\infty, \infty)$  which are integrable over every bounded interval. We call  $\{\delta_{\alpha}\}$  a delta sequence kernel of Dirichlet type if

1.  $\int_{-a}^a \delta_{\alpha} \rightarrow 1$  as  $\alpha \rightarrow \alpha_0$  for some finite constant  $a$ .
2. For every constant  $\gamma > 0$ ,  $(\int_{-\infty}^{-\gamma} + \int_{\gamma}^{\infty}) \delta_{\alpha} \rightarrow 0$  as  $\alpha \rightarrow \alpha_0$ .
3. There are positive constants  $C_1$  and  $C_2$  such that  $|\delta_{\alpha}(x)| \leq C_1/|x| + C_2$  for all  $x$  and  $\alpha$ .

Shannon's delta sequence kernel (or Dirichlet's continuous delta sequence kernel) is one of the most important examples of the delta sequence kernel of Dirichlet type and is given by the following (inverse) Fourier transform of the characteristic function,  $\chi_{[-\alpha/(2\pi), \alpha/(2\pi)]}$ :  $\delta_{\alpha}(x) = \int_{-\infty}^{\infty} \chi_{[-\alpha/(2\pi), \alpha/(2\pi)]} e^{-i2\pi\xi x} d\xi = \frac{\sin(\alpha x)}{\pi x}$ . Numerically, Shannon's delta sequence kernel is one of the most important cases because of its property of being an element of the Paley–Wiener reproducing kernel Hilbert space  $B_{1/2}^2$ ,

$$(2.4) \quad f(x) = \int_{-\infty}^{\infty} f(y) \frac{\sin \pi(x-y)}{\pi(x-y)} dy \quad \forall f \in B_{1/2}^2,$$

where  $\forall f \in B_{1/2}^2$  indicates that, in its Fourier representation, the  $L^2$  function  $f$  vanishes outside the interval  $[-\frac{1}{2}, \frac{1}{2}]$ . The Paley–Wiener reproducing kernel Hilbert space  $B_{1/2}^2$  is a subspace of the Hilbert space  $L^2(\mathbb{R})$ .

Shannon's delta sequence kernel is also known as a wavelet scaling function  $\phi(x) = \delta_{\pi}(x)$ . Shannon's mother wavelet can be constructed from the scaling function as  $\psi(x) = (\sin 2\pi x - \sin \pi x)/(\pi x)$ , with its Fourier expression,  $\hat{\psi}(\omega) = \chi_{[-1,1]}(\omega) - \chi_{[-1/2,1/2]}(\omega)$ . This is recognized as the ideal band pass filter and it satisfies the orthonormality conditions  $\sum_{n=-\infty}^{\infty} \hat{\psi}(\omega + n) = 1$  and  $\sum_{n=-\infty}^{\infty} |\hat{\psi}(\omega + n)|^2 = 1$ . Technically, it can be shown that a system of orthogonal wavelets is generated from a single function, the mother wavelet  $\psi$ , by standard operations of translation and dilation  $\psi_{mn}(x) = 2^{-(m/2)} \psi(\frac{x}{2^m} - n)$ ,  $m, n \in \mathbb{Z}$ .

Both  $\phi(x)$  and its associated wavelet play a crucial role in information theory and signal processing theory. However, their usefulness is limited by the facts that  $\phi(x)$  and  $\psi(x)$  are infinite impulse response (IIR) filters and their Fourier transforms  $\hat{\phi}(\omega)$  and  $\hat{\psi}(\omega)$  are not differentiable. From the computational point of view,  $\phi(x)$  and  $\psi(x)$  do not have finite moments in the coordinate space; in other words, they are delocalized. This nonlocal feature in the coordinate is related to their band-limited character in the Fourier representation by the Heisenberg uncertainty principle.

According to the theory of distributions, the smoothness, regularity, and localization of a temper distribution can be improved by a function of the Schwartz class. We apply this principle to regularize singular convolution kernels [23],

$$(2.5) \quad \delta_{\sigma,\alpha}(x) = R_\sigma(x)\delta_\alpha(x), \quad (\sigma > 0),$$

where  $R_\sigma$  is a *regularizer* which has properties

$$(2.6) \quad \lim_{\sigma \rightarrow \infty} R_\sigma(x) = 1, \quad R_\sigma(0) = 1.$$

Various delta regularizers can be used for numerical computations. A good example is the Gaussian  $R_\sigma(x) = \exp[-\frac{x^2}{2\sigma^2}]$ . The Gaussian regularizer is a Schwartz class function and has excellent numerical performance. However, we noted that, in certain eigenvalue problems, no regularization is required if the potential is smooth and bounded from below (e.g., the harmonic oscillator potential  $\frac{1}{2}x^2$ ).

In the rest of this subsection we describe the implementation of the DSC algorithm for the spatial discretization of PDEs. Without loss of generality, we consider a generic PDE of the form

$$(2.7) \quad \frac{\partial u}{\partial t} + \mathcal{L}u + F(u) = 0,$$

where  $F(u)$  is a source term and  $\mathcal{L}$  is a linear differential operator. In the DSC approach, it is convenient to discretize an operator on a grid of the coordinate representation and to use the collocation approach for solving a PDE [27]. Therefore, the source term can be discretized by  $[F(u)]_{x=x_m} = F(u_m)$ , where the (integer) subscript  $u_m$  denotes the spatial discretization of  $u$  with respect to the  $x$ -coordinate. The differential operator can be represented by the convolution

$$(2.8) \quad [\mathcal{L}u]_{x=x_m} = \sum_n d_n \left[ \frac{\partial^n u}{\partial x^n} \right]_{x=x_m} = \sum_n d_n \sum_{k=m-W}^{m+W} \delta_{\alpha,\sigma}^{(n)}(x_m - x_k) u_k,$$

where  $2W + 1$  is the computational bandwidth, or effective kernel support, and  $d_n$  is a coefficient. In (2.8),  $\delta_{\alpha,\sigma}^{(n)}(x_m - x_k)$  is *analytically* given in the DSC algorithm

$$(2.9) \quad \delta_{\alpha,\sigma}^{(n)}(x_m - x_k) = \left[ \left( \frac{d}{dx} \right)^n \delta_{\alpha,\sigma}(x - x_k) \right]_{x=x_m}.$$

The detailed expressions of these derivatives may be found in [29].

Therefore, a DSC semidiscrete form of the genetic equation can be expressed as

$$(2.10) \quad \frac{du_m}{dt} = - \sum_n d_n \sum_{k=m-W}^{m+W} \delta_{\alpha,\sigma}^{(n)}(x_m - x_k) u_k - F(u_m).$$

To take into account the temporal discretization, (2.10) can be rewritten in its vector form  $\frac{d\mathbf{u}}{dt} = \mathbf{G}_{\text{DSC}}(\mathbf{u}, t)$ , where  $\mathbf{u} = (u_1, u_2, \dots, u_m, \dots, u_N)$  and  $\mathbf{G}_{\text{DSC}}(\mathbf{u}, t)$  represents the DSC approximation in the right-hand side of (2.10).

For the time integration, the classical fourth-order Runge–Kutta (RK4) method is used to evaluate  $\mathbf{u}$  at each time step; i.e.,

$$(2.11) \quad \mathbf{u}^{j+1} = \mathbf{u}^j + \frac{1}{6}(\mathbf{r}_1 + 2\mathbf{r}_2 + 2\mathbf{r}_3 + \mathbf{r}_4),$$

in which

$$(2.12) \quad \mathbf{r}_1 = \Delta t \mathbf{G}_{\text{DSC}}(\mathbf{u}^j, t_j), \quad \mathbf{r}_2 = \Delta t \mathbf{G}_{\text{DSC}}\left(\mathbf{u}^j + \frac{1}{2}\mathbf{r}_1, t_j + \frac{1}{2}\Delta t\right),$$

$$(2.13) \quad \mathbf{r}_3 = \Delta t \mathbf{G}_{\text{DSC}}\left(\mathbf{u}^j + \frac{1}{2}\mathbf{r}_2, t_j + \frac{1}{2}\Delta t\right), \quad \mathbf{r}_4 = \Delta t \mathbf{G}_{\text{DSC}}(\mathbf{u}^j + \mathbf{r}_3, t_j + \Delta t).$$

**2.2. Accurate space derivatives.** The method of ASD introduced by Gazdag and Canosa [6] is commonly referred to as a pseudospectral method in the literature. The central point of the ASD method is that the incremental change  $\Delta u(x_n, t_m, \Delta t) = u_n^{m+1} - u_n^m$  is isolated into two parts of contribution,

$$(2.14) \quad \Delta u(x_n, t_m, \Delta t) = \Delta f(x_n, t_m, \Delta t) + \Delta g(x_n, t_m, \Delta t),$$

where  $\Delta f$  and  $\Delta g$  are the change in  $u$  due to diffusion and nonlinear reaction, respectively. At each time step,  $f$  and  $g$  are, respectively, the solution of

$$(2.15) \quad \frac{\partial f}{\partial t} = \frac{\partial^2 f}{\partial x^2} \quad \text{with} \quad f_n^m = u_n^m,$$

$$(2.16) \quad \frac{\partial g}{\partial t} = g(1 - g) \quad \text{with} \quad g_n^m = u_n^m.$$

To solve (2.15), the partial differentiation in the PDE is simply approximated by algebraic multiplications in spectral space as in other spectral methods. The time integration of (2.15) is exactly solved. By means of a truncated Taylor series, the solution of (2.16) can be obtained by successive differentiations of (2.16). Since the truncation order of the Taylor series is  $p = 4$ , Gazdag and Canosa argued that the temporal truncation error of the ASD scheme is  $O(\Delta t^{p+1}) = O(\Delta t^5)$ . In numerical studies, the ASD approach generates unexpected high frequency oscillations at the wave front, and an additional suppression procedure has to be employed to filter out these oscillations [6, 20, 2].

**2.3. Crank–Nicolson finite difference scheme.** Many different implicit finite difference schemes have been applied to Fisher's equation in the literature [8, 22, 13, 2]. In the present study, a linearized version of the CN finite difference scheme extended from a successful scheme for the logistic equation [22] is employed.

**2.4. Fourier pseudospectral method.** Spectral methods have been a popular choice for the numerical solution of various wave problems in recent years (see, for example, Fornberg [4, 5]). As global methods, the Fourier spectral methods usually are much more efficient than local methods (finite difference and finite element methods) for certain classes of nonlinear problems. In the present study, an FPS method of Sanders, Katoposes, and Boyd [19] is employed. In this scheme, a Fourier series is used in a collocation scheme and the time integration is obtained by using the RK4 method.

### 3. The analyses of spatial and temporal discretization errors.

**3.1. Discrete Fourier analysis of spatial approximation resolution.** In this subsection, we will briefly conduct a discrete Fourier analysis of the spatial approximation resolution associated with the DSC approach. The analysis of the CN scheme can be carried out similarly, since the present DSC approach can be viewed as a simple, systematic algorithm for the generation of finite difference schemes of an

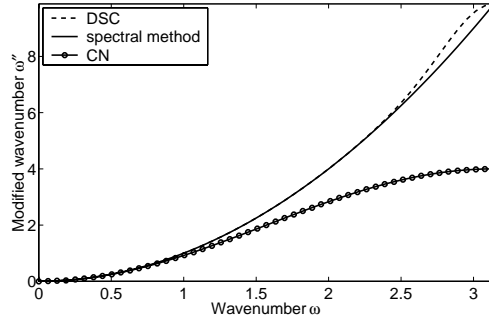


FIG. 3.1. Plot of absolute values of modified wavenumbers versus wavenumber for second derivative approximation.

arbitrary order [27]. For a more detailed Fourier analysis of the numerical resolution of the DSC algorithm, we refer to [33].

Fourier analysis is a classical technique for comparing different schemes [21]. Indeed, discrete Fourier analysis characterizes the Fourier resolution of an interpolation or differentiation scheme applied to a class of compactly supported and periodic functions. Thus, Fourier analysis is capable of providing an effective way to quantify the accuracy of different approximation schemes used for band-limited periodic functions. It is noted that the outcome of the analysis may not hold when the function is not band limited and periodic.

Because the derivatives are approximated by means of discrete convolution (see (2.8)) in the DSC algorithm, according to the convolution theorem, the corresponding Fourier coefficients of spatial derivatives can be expressed as  $\hat{u}_k^{(n)} = \hat{\delta}_{\alpha,\sigma}^{(n)}(k)\hat{u}_k$ , where  $\hat{\delta}_{\alpha,\sigma}^{(n)}(k) = \frac{1}{N} \sum_{j=0}^{N-1} \delta_{\alpha,\sigma}^{(n)}(x_j) \exp(-i\xi_k x_j)$ . Here, by using resolution  $\Delta = L/N$ , the discrete wavenumbers  $\xi_k = 2\pi k/L$  ( $k = -N/2 + 1, \dots, -1, 0, 1, \dots, N/2$ ) range from  $-\pi/\Delta$  to  $\pi/\Delta$ . The quantity  $\pi/\Delta$  is the Nyquist frequency, which is the maximum wavenumber that could be distinguished by the discretization with the mesh size  $\Delta$ . Any wavenumber whose absolute value is greater than the Nyquist frequency will be misinterpreted and contribute to the aliasing error. For convenience, we introduce a scaled wavenumber  $\omega = 2\pi k\Delta/L = 2\pi k/N$  and a scaled coordinate  $s = x/\Delta$ . In terms of these new definitions, the Fourier modes are simply  $\exp(-i\omega x)$  and the domain of the wavenumber  $\omega$  is  $[-\pi, \pi]$ .

Generally, the derivative approximation of different schemes can be expressed in the spectral space in a unified form,  $\hat{u}_k^{(n)} = \omega^{(n)}\hat{u}_k$ . For the second-order derivative, both the FPS and ASD methods provide the exact response function  $\omega^{(2)} = -\omega^2$  within the frequency band  $[-\pi, \pi]$ . It is noted that other spectral methods do not provide exact derivatives with respect to the discrete Fourier analysis. For the DSC and CN schemes, the accuracy of the derivative approximations for band-limited periodic functions can be indicated by the closeness of the modified wavenumber  $\omega^{(2)}$  to  $-\omega^2$ ; see Figure 3.1. It is obvious from Figure 3.1 that the DSC scheme can stay very close to the exact differentiation except for very high wavenumbers, while the central finite difference used in the CN scheme deviates from the exact second derivative very quickly.

The analysis indicates that the spectral basis provides the most accurate (i.e., exact) representation in the Fourier space. However, the same spectral basis is not



the best basis in a finite polynomial space, where the finite difference approximation can be proved to be the most accurate basis. The analysis also reveals that the DSC algorithm provides extremely high accuracy comparable to the pseudospectral method for approximating band-limited periodic functions. In fact, for problems with some other features, the DSC algorithm can be more accurate than the pseudospectral method [33].

**3.2. Temporal discretization errors.** The standard temporal discretizations are used for the CN, FPS, and DSC schemes. Thus, it is clear that the temporal discretization error is of fourth order for both the FPS and DSC schemes and is  $O(\Delta t^2)$  for the CN scheme. The time truncation error for the ASD scheme needs to be clarified, although it was stated as  $O(\Delta t^5)$  [6].

Substitute the initial conditions in (2.15) and (2.16) at time step  $t_m$  into (2.14),

$$(3.1) \quad \Delta u(x_n, t_m, \Delta t) = u_n^{m+1} - u_n^m = f_n^{m+1} - u_n^m + g_n^{m+1} - u_n^m.$$

Consequently, we have

$$(3.2) \quad u_n^{m+1} = f_n^{m+1} + g_n^{m+1} - u_n^m.$$

Consider the temporal semidiscretization form of (1.2), i.e., the integral of

$$(3.3) \quad u_n^{m+1} - u_n^m = \int_{t_m}^{t_{m+1}} \frac{\partial^2 u(x_n, s)}{\partial x^2} ds + \int_{t_m}^{t_{m+1}} u(x_n, s)(1 - u(x_n, s)) ds.$$

Instead of solving (3.3), the ASD scheme actually solves

$$(3.4) \quad \begin{aligned} f_n^{m+1} - u_n^m &= \int_{t_m}^{t_{m+1}} \frac{\partial^2 f(x_n, s)}{\partial x^2} ds, \\ g_n^{m+1} - u_n^m &= \int_{t_m}^{t_{m+1}} g(x_n, s)(1 - g(x_n, s)) ds. \end{aligned}$$

In terms of the same discrete numerical temporal integration method, (3.3) and (3.4) are equivalent only if the conditions

$$(3.5) \quad f_n^{m+1} = u_n^{m+1}, \quad g_n^{m+1} = u_n^{m+1}$$

are satisfied simultaneously. This is not true due to (3.2), and these important conditions are neglected in the formulation of the ASD scheme. Conditions (3.5) can be approximately satisfied when  $\Delta t \rightarrow 0$ ,

$$(3.6) \quad f_n^{m+1} = u_n^{m+1} + O(\Delta t), \quad g_n^{m+1} = u_n^{m+1} + O(\Delta t).$$

Therefore, the temporal truncation error of the ASD scheme is  $O(\Delta t)$ . This is verified by the numerical experiments reported in the next section.

**4. Numerical studies.** In the present study, we focus our attention on a particular DSC kernel, the regularized Shannon's kernel, which has been extensively used in previous calculations [23, 24, 25, 26, 27, 28, 29, 30, 31, 32, 33]. The DSC parameters are chosen as  $W = 32$  and  $\sigma = 3.5\Delta$  [24]. For the FPS and ASD methods, the computational domain is symmetrically extended so that the periodic BC can be assumed [6]. Thus, for the two spectral methods, when mesh points are reported as  $N$ , there are actually  $2N$  grid points used in the computation.

To make a detailed comparison of the DSC, CN, FPS, and ASD methods, several Cauchy problems of Fisher's equation, with or without analytical solutions, are employed. The initial wave profiles studied are all of SSW type. The following SSW solution is employed in the numerical studies of Li, Petzold, and Ren [11] and Qiu and Sloan [16]:

$$(4.1) \quad u(x, t) = \left[ 1 + \exp \left( \sqrt{\frac{\rho}{6}} x - \frac{5\rho}{6} t \right) \right]^{-2}.$$

This traveling wave solution satisfies a scaled Fisher's equation,

$$(4.2) \quad \frac{\partial u}{\partial t} = \frac{\partial^2 u}{\partial x^2} + \rho u(1 - u),$$

and nonlocal conditions (1.3) and (1.4). The speed of the solution (4.1) is  $c = 5\sqrt{\rho/6}$ . For the numerical studies of solution (4.1), the accuracy of the numerical results is measured by means of the  $L_\infty$ - and  $L_2$ -norms. Here  $L_\infty = \max_{i=1, \dots, N} |\hat{u}_i - u_i|$  and  $L_2 = [\frac{1}{N} \sum_{i=1}^N (\hat{u}_i - u_i)^2]^{1/2}$ , where  $u_i$  and  $\hat{u}_i$  are the analytical and numerical solutions, respectively.

Apart from SSW solution (4.1), other types of SSW profiles are also studied. For the purpose of general applications, the difference of the theoretical and numerical wave speed  $|c - \hat{c}|$  is calculated for all studied cases. To estimate the speed of the simulated traveling wave solution,  $\hat{c}$ , a reference position for the propagating wave front is introduced,  $x_f^m = \int_{x_L}^{x_R} u(x, t_m) dx$ . This reference position is a simpler version of that used by Carey and Shen [2], and the integral is approximated by using Simpson's rule. By using this estimate of wave front location, the wave speed may be approximated as  $c^m = (x_f^m - x_f^{m-1})/\Delta t$ . Note that the wave speed difference,  $|c - \hat{c}|$ , can be explained as an approximation error only when the solution reaches the steady state of the motion.

**4.1. Weak reaction problem.** We first consider  $\rho = 1$  in solution (4.1); (4.2) then is identical to (1.2). The wave speed of the analytical solution is  $c = 5\sqrt{1/6} \approx 2.04124 > 2$ . Fisher's equation is numerically solved via the four methods. Because the BC applied on the left-hand boundary is relatively unimportant to the correctness of the numerical solutions, throughout the present work, the BC on the left is fixed as the Dirichlet BC by setting  $u(x_L, t) = 1$  in the DSC and CN schemes. Since the FPS and ASD methods can be used only for periodic BCs, the *exact* BC (i.e., the BC given by the exact solution (4.1)) used in [11, 16] cannot be directly implemented for the FPS and ASD methods. To achieve a comparison of the four methods, we apply the *zero* BC (the Dirichlet BC by setting  $u(x_R, t) = 0$ ) at the right-hand boundary in the DSC and CN schemes.

The numerical results approximated by the four numerical approaches with different resolutions are listed in Table 4.1. It can be seen from Table 4.1 that the DSC algorithm always has accuracy comparable to the FPS method, and both schemes achieve very high accuracy. However, for the ASD method, although highly accurate spatial discretization is used, the approximated results are much less accurate than those of the FPS. When  $\Delta t$  is large, the results of the ASD are even worse than those of the CN.

To numerically test the order of accuracy of each scheme with respect to spatial and temporal discretizations, the used resolutions in Table 4.1 are specially designed. A general principle is that, to test the spatial (or temporal) accuracy order, the

TABLE 4.1

Comparison of numerical solution of a scaled Fisher's equation with  $\rho = 1$  by using the DSC, CN, FPS, and ASD schemes.

Scheme	$N$	$\Delta x$	$\Delta t$	$t = 5.0$			$t = 10.0$		
				$L_\infty$	$L_2$	$ c - \hat{c} $	$L_\infty$	$L_2$	$ c - \hat{c} $
DSC	128	1.0	0.2	1.34(-5)	2.74(-6)	4.25(-5)	5.61(-5)	1.17(-5)	9.15(-5)
	128	1.0	0.1	9.00(-7)	1.84(-7)	2.95(-6)	3.86(-6)	8.03(-7)	6.41(-6)
	64	2.0	0.01	4.35(-6)	9.38(-7)	1.34(-7)	3.12(-6)	6.50(-7)	1.19(-7)
	128	1.0	0.01	1.59(-9)	2.50(-10)	7.02(-9)	1.39(-9)	2.06(-10)	8.43(-10)
CN	512	0.25	0.2	5.18(-3)	1.10(-3)	1.18(-2)	1.43(-2)	2.99(-3)	1.69(-2)
	512	0.25	0.1	1.35(-3)	2.91(-4)	3.48(-3)	4.25(-3)	8.88(-4)	5.53(-3)
	64	2.0	0.01	1.02(-2)	1.87(-3)	4.47(-2)	5.47(-2)	1.16(-2)	1.04(-1)
	128	1.0	0.01	2.66(-3)	4.84(-4)	1.15(-2)	1.46(-2)	3.06(-3)	2.77(-2)
FPS	128	1.0	0.2	1.34(-5)	2.74(-6)	4.25(-5)	5.61(-5)	1.17(-5)	9.15(-5)
	128	1.0	0.1	9.01(-7)	1.84(-7)	2.94(-6)	3.86(-6)	8.03(-7)	6.41(-6)
	64	2.0	0.01	3.16(-6)	6.75(-7)	6.89(-8)	3.21(-6)	6.76(-7)	1.10(-7)
	128	1.0	0.01	1.27(-9)	1.38(-10)	4.01(-9)	4.40(-10)	8.78(-11)	7.58(-10)
ASD	128	1.0	0.2	3.84(-2)	7.24(-3)	9.38(-2)	1.09(-1)	2.19(-2)	1.26(-1)
	128	1.0	0.1	1.96(-2)	3.73(-3)	4.93(-2)	5.62(-2)	1.14(-2)	6.68(-2)
	64	2.0	0.01	1.99(-3)	3.83(-4)	5.16(-3)	5.67(-3)	1.18(-3)	7.06(-3)
	128	1.0	0.01	1.99(-3)	3.83(-4)	5.16(-3)	5.72(-3)	1.18(-3)	7.06(-3)

TABLE 4.2

Numerically tested accuracy order of the four methods.

Halve	$t = 5.0$				$t = 10.0$			
	DSC	CN	FPS	ASD	DSC	CN	FPS	ASD
$\Delta t$	3.89	1.92	3.89	0.96	3.86	1.75	3.86	0.94
$\Delta x$	11.87	1.95	12.26	3.77(-5)	11.62	1.92	12.91	1.22(-4)

temporal (spatial) resolution will be chosen as sufficiently fine and kept unchanged, while the spatial (temporal) resolution will be halved. The principle is easily satisfied for testing spatial accuracy by setting  $\Delta t = 0.01$  and halving  $\Delta x = 2.0$  to 1.0. For testing temporal accuracy, however,  $\Delta x$  could not be too small, because usually there is a stability constraint for the mesh ratio  $\Delta t/\Delta x^2$  for explicit schemes. Fortunately, the spatial discretization accuracy of three explicit schemes, the DSC, the FPS, and the ASD, is very high such that  $\Delta x = 1.0$  is enough in the present study to guarantee that the approximation errors are mainly contributed by the temporal discretization. For the low spatial accuracy scheme, the CN,  $\Delta x$  is set to  $\Delta x = 0.25$ , since the CN scheme is unconditionally stable.

In terms of the  $L_2$  errors, the error decreasing rates of each scheme are recalculated from Table 4.1 and are presented in Table 4.2. The numerically estimated accuracy orders are all in excellent agreement with the theoretical analyses in section 3. When  $\Delta x$  is halved, the DSC results become over 3000 times more accurate than the original ones, and the accuracy increasing rates of the FPS are even larger than 4000. The numerical results indicate that the spatial accuracy orders of these two schemes are extremely high. The temporal discretization orders of both the DSC and FPS schemes are approximately  $O(\Delta t^4)$ , since the same RK4 scheme is used in both schemes. The numerically tested truncation errors of the CN scheme are also in agreement with the classic theoretical analysis, i.e.,  $O(\Delta x^2)$  and  $O(\Delta t^2)$ . It is interesting to note that by halving  $\Delta x$ , the accuracy of the ASD results remains unchanged; this means that the approximation errors of the ASD scheme are fully introduced by temporal discretization. By halving  $\Delta t$ , the accuracy of the ASD results increases approximately two times; therefore, the temporal truncation error of the ASD scheme

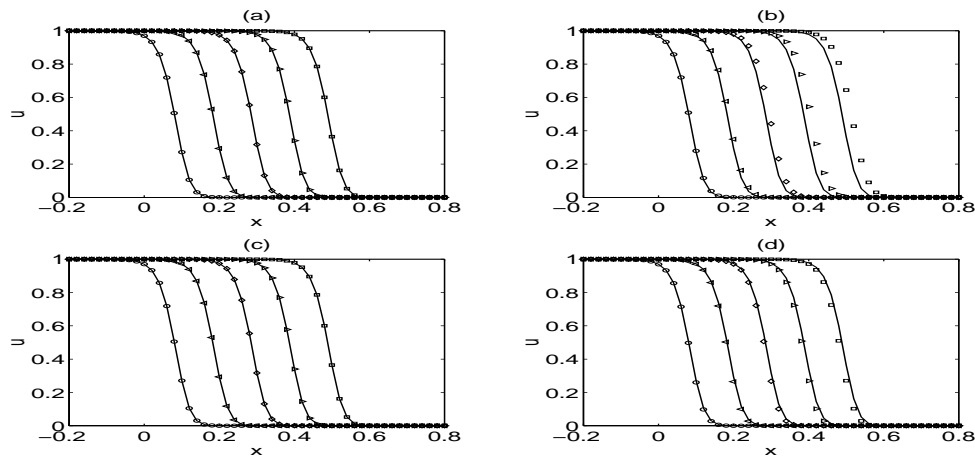


FIG. 4.1. Numerical solutions of a scaled Fisher's equation with  $\rho = 10^4$  at times  $t = 5.0(-4)$ ,  $1.0(-3)$ ,  $\dots$ ,  $2.5(-3)$ . (a) The DSC solutions; (b) the CN solutions; (c) the FPS solutions; (d) the ASD solutions. In all charts, the continuous lines represent the analytical solutions at the corresponding times.

is  $O(\Delta t)$ . This verifies the earlier analysis.

**4.2. Strong reaction problem.** The strong reaction problem,  $\rho = 10^4$ , is considered for the scaled Fisher's equation (4.2). The wave speed of the analytical solution is  $c = 5\sqrt{10^4/6} \approx 204.124$ . It is noted that this wave speed is in terms of the unnormalized coordinate system. The corresponding minimum wave speed is  $c = 200$ .

**4.2.1. Shock-like wave.** With the strong reaction force, the solution evolves into a shock-like wave. Thus, in order to properly represent the rapidly changing solution by a low-order scheme, very fine resolution has to be used. To avoid the burden of using a large computation grid, a nonuniform mesh is conventionally used. Li, Petzold, and Ren [11] and Qiu and Sloan [16] considered this strong reaction problem by using the moving mesh methods, which are able to redistribute grid points to follow a rapidly changing solution. Satisfactory results were obtained in [16].

In the present study, we consider a uniform mesh to solve this strong reaction problem. Following the discrete Fourier analysis in section 3, higher-order schemes are much better in resolving a higher wavenumber, with the same spacing  $\Delta x$ . Therefore, an accurate result could be obtained by using higher-order schemes with small  $N$ . To illustrate this argument, the solution of Fisher's equation with  $\rho = 10^4$  is approximated by the DSC, CN, FPS, and ASD schemes. The zero BC is used in both the DSC and CN schemes. Discretization parameters used here are similar to those of [16]:  $N = 64$ ,  $\Delta x = 0.02$ , and  $\Delta t = 5.0(-6)$ . The computation domain is fixed as  $[x_L, x_R] = [-0.2, 1.06]$ . Note that the present mesh resolution is equal to the average mesh resolution used in [16]. The present numerical results are shown in Figure 4.1 and Table 4.3. It can be seen from Table 4.3 that the results of moving mesh methods are much more accurate than those of the convention finite difference scheme, while the results of higher-order schemes, i.e., the FPS and DSC, are in turn much more accurate than those in [16]. However, for the FPS scheme, although a very accurate result is obtained up to  $t = 2.5(-3)$ , it blows up at  $t = 4.0(-3)$ .

As noticed by some researchers [6, 20, 2] in the literature, spectral methods generate unwanted oscillations at the wave front, and since the solution of Fisher's equation

TABLE 4.3

Comparison of short-term solution of a scaled Fisher's equation with  $\rho = 10^4$  approximated by the DSC, CN, FPS, and ASD schemes and by moving mesh methods. Three results from Qiu and Sloan [16] are listed. (a) MMDAE with  $N = 50$ ; (b) MMPDE6 with  $N = 50$  and  $\tau = 10^{-7}$ ; (c) method of lines on an evenly spaced grid with  $N = 300$ .

Scheme	Error	$t$							
		5.0(-4)	1.0(-3)	1.5(-3)	2.0(-3)	2.5(-3)	3.0(-3)	3.5(-3)	4.0(-3)
DSC	$L_\infty$	6.28(-6)	3.03(-6)	1.98(-6)	3.23(-6)	4.46(-6)	5.44(-6)	6.22(-6)	1.69(-5)
	$L_2$	1.24(-6)	6.53(-7)	5.92(-7)	8.35(-7)	1.16(-6)	1.43(-6)	1.64(-6)	4.30(-6)
	$ c - \hat{c} $	2.53(-3)	1.06(-4)	6.23(-5)	6.58(-5)	7.37(-5)	1.00(-4)	5.19(-4)	1.57(-2)
CN	$L_\infty$	1.03(-2)	5.55(-2)	1.25(-1)	2.04(-1)	2.80(-1)	3.60(-1)	4.48(-1)	5.21(-1)
	$L_2$	1.92(-3)	1.17(-2)	2.65(-2)	4.36(-2)	6.18(-2)	8.04(-2)	9.91(-2)	1.17(-1)
	$ c - \hat{c} $	4.49(+0)	1.04(+1)	1.31(+1)	1.46(+1)	1.54(+1)	1.60(+1)	1.64(+1)	1.67(+1)
FPS	$L_\infty$	3.13(-6)	3.47(-6)	3.90(-6)	5.00(-6)	7.82(-5)	4.23(-3)	3.42(-1)	$\infty$
	$L_2$	7.71(-7)	6.79(-7)	7.02(-7)	9.04(-7)	2.11(-5)	1.19(-3)	8.95(-2)	$\infty$
	$ c - \hat{c} $	1.58(-3)	7.72(-5)	9.73(-5)	1.87(-3)	9.68(-2)	5.54(+0)	4.76(+2)	$\infty$
ASD	$L_\infty$	1.07(-2)	2.88(-2)	4.93(-2)	7.10(-2)	9.37(-2)	1.24(-1)	9.44(-1)	$\infty$
	$L_2$	2.09(-3)	6.07(-3)	1.06(-2)	1.53(-2)	2.02(-2)	2.68(-2)	2.35(-1)	$\infty$
	$ c - \hat{c} $	2.61(+0)	3.45(+0)	3.70(+0)	3.80(+0)	4.05(+0)	1.59(+1)	3.41(+2)	$\infty$
[16] (a)	$L_\infty$					9.25(-3)			
[16] (b)	$L_\infty$					4.29(-2)			
[16] (c)	$L_\infty$					9.34(-3)			

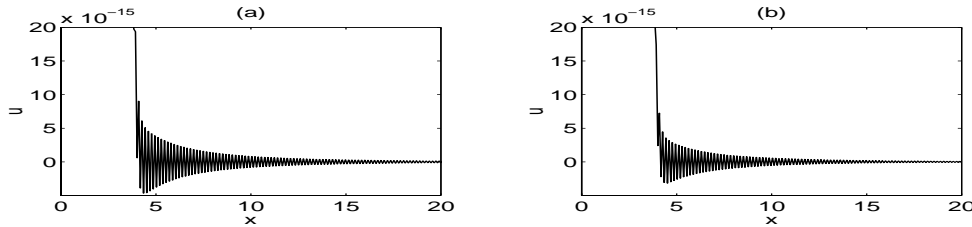


FIG. 4.2. The plots of the front parts of the wave solutions approximated by the FPS and ASD schemes at time  $t = 1\Delta t$ . (a) The FPS solution; (b) the ASD solution.

is unstable to the small perturbation at the wave front, the results of spectral methods quickly become unstable. In the present studies, it is found that the serious oscillations are generated in both the FPS and ASD solutions even after only one time integration (see Figure 4.2), while the DSC and CN results are free of these oscillations. To ensure the stability, Gazdag and Canosa [6] suggested using an additional procedure to suppress the oscillations at each time step; i.e., if  $u(x_n, t_m) \leq \epsilon$ , then  $u(x_n, t_m) = 0$ . Here the threshold  $\epsilon$  is a small positive number and is chosen empirically. Note that by adopting this suppression procedure, it is equivalent to imposing the zero BC at  $x_R(t_m)$ .

**4.2.2. The moving frame method.** In order to simulate the long-time behavior of the traveling wave solutions, the computational domain has to be very large due to the high wave speed. At the same time, a relatively fine spatial resolution is required to properly represent the wave solution of this strong reaction problem. Therefore, the computational cost will be extremely expensive, as much computation is wasted on unimportant regions. To reduce the computational cost, a moving coordinate system with user-specified speed was introduced by Hagstrom and Keller [8]: at each instant, the computation is focused only on a narrow region within the frame. However, this technique could not be directly applied to general cases since,

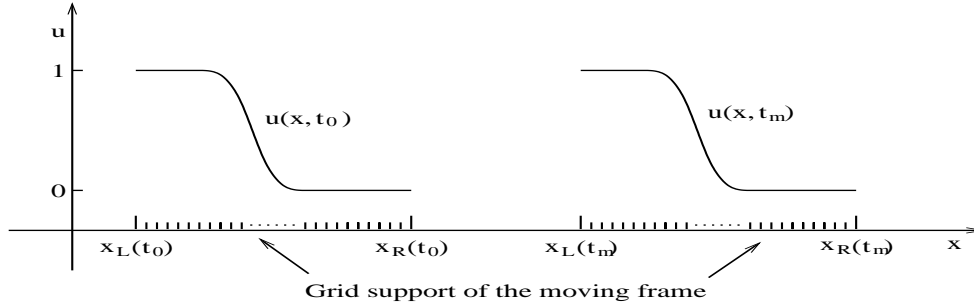


FIG. 4.3. The schematic plot of the moving frame coordinate.

in practice, the speed of the moving coordinate system may not be known a priori.

To account for wide applications, a moving frame method is introduced in the present study. The method provides grid support only to the region of interest. The center of the moving frame goes along with the center of the traveling wave. As such, the moving frame method dramatically reduces the computational grid size. To this end, we introduce a monitor function

$$(4.3) \quad M(x, t) = \sqrt{\phi^2 + \psi^2 (\partial u(x, t) / \partial x)^2}.$$

Monitor function (4.3) can be viewed as a generalization of the arc-length monitor function, which is widely used in moving mesh methods [11, 16]. Then the central point of the traveling wave solution can be identified by means of the monitor function (4.3),  $x_c^m = \max_{n=1,2,\dots,N} M(x_n, t_m)$ . In the numerical study, the initial computation domain,  $[x_L(t_0), x_R(t_0)]$ , is first selected and the initial wave center,  $x_c^0$ , is calculated. Then the computational domain will move according to the corresponding wave center, i.e.,  $x_L(t_m) = x_L(t_0) + (x_c^m - x_c^0)$ , and  $x_R(t_m) = x_R(t_0) + (x_c^m - x_c^0)$ , at each time step  $t_m$ . It is noted that the objectives of the present moving frame method and the previous moving mesh method [11, 16] are different; e.g., the former moves the coordinate system to follow up a rapidly traveling solution (see Figure 4.3), while the latter seeks a redistribution of grid points to catch up with a rapidly changing solution within a fixed coordinate system. A uniform mesh with a fixed resolution is used in the moving frame method. If  $x_R(t_m) > x_R(t_{m-1})$ , then  $u(x_R(t_m), t_m)$  will be given by the BC applied on  $x_R(t_m)$ . In the present study, for simplicity we choose  $\phi = 0$  and  $\psi = 1$ , although  $\phi = 1$  could also be utilized.

In association with the moving frame method, the medium-term solutions of the scaled Fisher's equation are approximated by the four methods. For all four methods, the spatial discretization parameters are fixed as  $N = 512$  and  $\Delta x = 8.5(-3)$ , and the time increment is set to  $\Delta t = 5.0(-6)$ . The zero BC is applied at the right boundary in the DSC and CN schemes; the empirically optimal threshold is chosen to suppress the oscillations in two spectral methods. The numerical results are presented in Table 4.4. It can be seen from Table 4.4 that the steady states of motion are reached for the numerical solutions of the CN, FPS, and ASD methods. The asymptotic velocities of these solutions are all incorrect. The steady state wave speed of the FPS results is  $c = 199.5 \approx 200$ , which is close to the expectation of the theoretical analysis while, for two low accuracy methods (the CN and ASD), the asymptotic velocities have very large errors. The wave speed estimated by the FPS and ASD methods with optimal suppression is shown in Figure 4.4. The results of the DSC approach are

TABLE 4.4

Comparison of medium-term solution of a scaled Fisher's equation with  $\rho = 10^4$  approximated by the DSC, CN, FPS, and ASD schemes.

Scheme	Error	$t$					
		0.02	0.04	0.06	0.08	0.10	0.12
DSC, zero BC	$L_\infty$	1.74(-5)	3.57(-5)	6.21(-5)	1.57(-2)	2.07(-1)	7.66(-1)
	$L_2$	1.97(-6)	4.07(-6)	7.05(-6)	1.78(-3)	2.36(-2)	9.94(-2)
	$ c - \hat{c} $	7.70(-5)	7.72(-5)	4.84(-4)	2.66(-1)	1.40(+0)	1.62(+1)
CN, zero BC	$L_\infty$	6.54(-1)	9.30(-1)	9.88(-1)	9.98(-1)	1.00(+0)	1.00(+0)
	$L_2$	8.23(-2)	1.46(-1)	1.93(-1)	2.30(-1)	2.62(-1)	2.88(-1)
	$ c - \hat{c} $	3.45(+0)	3.45(+0)	3.45(+0)	3.45(+0)	3.31(+0)	2.95(+0)
CN, exact BC	$L_\infty$	6.54(-1)	9.30(-1)	9.88(-1)	9.98(-1)	1.00(+0)	1.00(+0)
	$L_2$	8.23(-2)	1.46(-1)	1.93(-1)	2.30(-1)	2.62(-1)	2.89(-1)
	$ c - \hat{c} $	3.45(+0)	3.45(+0)	3.45(+0)	3.45(+0)	3.35(+0)	3.02(+0)
CN, asymptotic BC	$L_\infty$	6.54(-1)	9.30(-1)	9.88(-1)	9.98(-1)	1.00(+0)	1.00(+0)
	$L_2$	8.23(-2)	1.46(-1)	1.93(-1)	2.30(-1)	2.62(-1)	2.89(-1)
	$ c - \hat{c} $	3.45(+0)	3.45(+0)	3.45(+0)	3.45(+0)	3.35(+0)	3.02(+0)
FPS, $\epsilon = 1.0(-14)$	$L_\infty$	6.75(-1)	9.64(-1)	9.97(-1)	9.99(-1)	1.00(+0)	1.00(+0)
	$L_2$	8.46(-2)	1.64(-1)	2.19(-1)	2.63(-1)	3.00(-1)	3.33(-1)
	$ c - \hat{c} $	4.57(+0)	4.58(+0)	4.58(+0)	4.58(+0)	4.58(+0)	4.58(+0)
ASD, $\epsilon = 1.5(-14)$	$L_\infty$	9.58(-1)	9.99(-1)	1.00(+0)	1.00(+0)	1.00(+0)	1.00(+0)
	$L_2$	1.59(-1)	2.55(-1)	3.24(-1)	3.80(-1)	4.29(-1)	4.73(-1)
	$ c - \hat{c} $	8.62(+0)	8.66(+0)	8.65(+0)	8.65(+0)	8.65(+0)	8.65(+0)

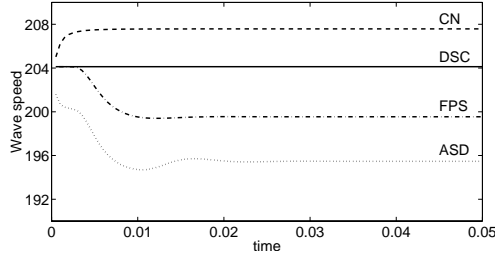


FIG. 4.4. The plots of the wave speed estimated by four methods for the strong reaction problem.

more accurate than others, as shown in Table 4.4. However, the final DSC results are also relatively inaccurate, which is due to the improper BC.

**4.2.3. A new asymptotic scheme.** Apart from the exact BC, the only proper BC reported in the literature is the one given by Hagstrom and Keller [8]. In the present study, however, their BC is relatively complicated to implement. Therefore, a simple *asymptotic* BC is introduced that is based on a consideration similar to that in [8]. By assuming that the solution at the boundary cutoff is sufficiently close to its limiting value, an asymptotic representation of the initial data in the discarded region can be simply expressed as

$$(4.4) \quad u_0(x) = \tilde{a} \exp(-\tilde{b}x), \quad x \geq x_R(t_0),$$

for some constants  $\tilde{a}$  and  $\tilde{b}$ . When  $x$  is sufficiently large, the finite sum of exponentials for the initial data used in [8] can be well approximated by (4.4). Furthermore, when  $x \rightarrow \infty$ ,  $\tilde{b}$  will tend to  $\beta$ . Without cumbersome construction, the asymptotic BC utilized in the present work is assumed to have the form

$$(4.5) \quad u(x, t_m) = \tilde{a} \exp(-\tilde{b}(x - \tilde{c}t_m)), \quad x \geq x_R(t_m),$$

TABLE 4.5

Long-term solution of a scaled Fisher's equation with  $\rho = 10^4$  approximated by the DSC scheme.

$t$	DSC, exact BC			DSC, asymptotic BC		
	$L_\infty$	$L_2$	$ c - \hat{c} $	$L_\infty$	$L_2$	$ c - \hat{c} $
0.02	1.74(-5)	1.97(-6)	7.70(-5)	1.74(-5)	1.97(-6)	7.70(-5)
0.04	3.57(-5)	4.07(-6)	7.72(-5)	3.57(-5)	4.07(-6)	7.72(-5)
0.06	5.43(-5)	6.16(-6)	7.71(-5)	5.43(-5)	6.16(-6)	7.71(-5)
0.08	4.05(-5)	4.59(-6)	5.68(-4)	4.05(-5)	4.59(-6)	5.68(-4)
0.10	3.11(-4)	3.53(-5)	1.53(-3)	3.11(-4)	3.53(-5)	1.53(-3)
0.20	4.84(-4)	5.49(-5)	3.12(-5)	4.84(-4)	5.49(-5)	3.12(-5)
0.30	4.87(-4)	5.53(-5)	3.69(-5)	4.87(-4)	5.53(-5)	3.69(-5)
0.40	4.90(-4)	5.57(-5)	3.81(-5)	4.90(-4)	5.57(-5)	3.81(-5)
0.50	4.94(-4)	5.60(-5)	1.31(-5)	4.94(-4)	5.60(-5)	1.31(-5)
0.60	4.91(-4)	5.60(-5)	1.09(-5)	4.91(-4)	5.60(-5)	1.09(-5)
0.70	4.92(-4)	5.57(-5)	2.22(-5)	4.92(-4)	5.57(-5)	2.22(-5)
0.80	4.94(-4)	5.65(-5)	3.68(-5)	4.94(-4)	5.65(-5)	3.68(-5)
0.90	4.89(-4)	5.54(-5)	1.17(-5)	4.89(-4)	5.54(-5)	1.17(-5)
1.00	4.88(-4)	5.57(-5)	2.99(-5)	4.88(-4)	5.57(-5)	2.99(-5)

for each time step  $t_m$ . Unlike the BC in [8], where the asymptotic expansion is assumed to be known, here the constants  $\tilde{a}$ ,  $\tilde{b}$ , and  $\tilde{c}$  are estimated from initial data at the boundary cutoff  $x_N = x_R(t_0)$ ,

$$(4.6) \quad \begin{aligned} \tilde{a} &= \frac{u_0(x_N)}{\exp(-x_N \ln(u_0(x_{N-1})/u_0(x_N))/\Delta x)}, \\ \tilde{b} &= \ln(u_0(x_{N-1})/u_0(x_N))/\Delta x, \end{aligned}$$

$$(4.7) \quad \tilde{c} = \begin{cases} \tilde{b} + \frac{1}{\tilde{b}}, & \tilde{b} \leq 1, \\ 2, & \tilde{b} \geq 1. \end{cases}$$

In other words, the asymptotic BC is self-contained in our numerical algorithm; no additional knowledge about the initial data is requested in advance. Therefore, the advantages of the present asymptotic BC are that it is simple, fully automatic, and suitable for general applications.

By using the asymptotic and exact BCs at  $x = x_R$ , the long-term solutions of Fisher's equation are approximated via the DSC algorithm; see Table 4.5. It is obvious that the asymptotic BC results are the same as those of the exact BC, which means that the proposed asymptotic BC approximates the exact BC extremely well. The steady state solutions are reached at  $t = 0.2$ ; the final DSC results are very accurate at  $t = 1.0$ . In fact, similarly accurate results can be obtained no matter how large  $t$  is. The asymptotic and exact BCs can be implemented with the CN scheme; the corresponding results are contained in Table 4.4. However, no improvement is made in the CN results by using either the asymptotic or exact BC. The uselessness of the asymptotic and exact BCs here is due to the low accuracy of the CN scheme for this problem. The wave speeds estimated by the DSC and CN schemes with the asymptotic BC are depicted in Figure 4.4.

Therefore, apart from the appropriate BC, the accuracy of the scheme is also a crucial factor for producing correct results. For the strong reaction problem, only the highly accurate DSC schemes can give the results as predicted by theoretical analysis; see Figure 4.5. It can be seen from Figure 4.5 that the wave solution of the FPS has a speed of  $c \approx 200$ . The importance of the moving frame method is also clearly



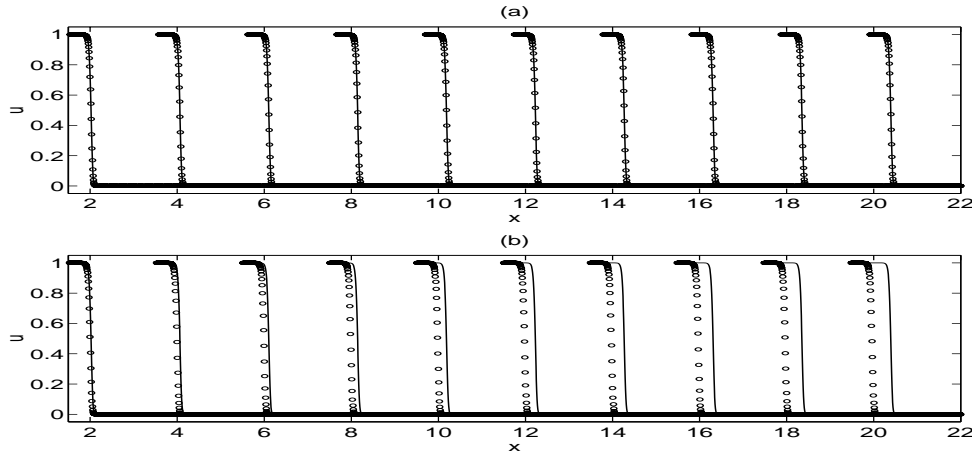


FIG. 4.5. Numerical solutions of a scaled Fisher's equation with  $\rho = 10^4$  at times  $t = 0.01, 0.02, \dots, 0.1$ . (a) The DSC solutions; (b) the FPS solutions. In both charts, the continuous lines represent the analytical solutions at the corresponding times.

illustrated in Figure 4.5. It is seen that the frame moves consistently according to the simulated wave speed and, at each instant, the computational domain is very narrow compared with the whole occupied physical domain.

**4.3. SSW simulation study.** In this subsection, we study further the sensitivity of the simulated speed of the traveling wave to the proper BCs. In addition to the wave solution (4.1), there are other kinds of SSW solutions studied in the literature [1, 6, 8, 2]. Since Hagstrom and Keller did not explicitly report their initial wave profiles, the only available example of an initial SSW profile is the one given by Canosa [1], which was also considered by other authors [6, 2]. Unfortunately, as reported by Carey and Shen [2], a slight negative undershoot appears in the initial profile of such an SSW so that a noticeably negative undershoot will be developed in the computation. Carey and Shen suggest forcing the negative  $u$  to zero in the initial profile. However, by doing so, the initial wave profile will evolve into a minimum speed wave.

In the present study, the dimensionless Fisher's equation (1.2) is considered and several SSW profiles are simply generated by the initial function

$$(4.8) \quad u_0(x) = [1 + \exp(b_1x) + \exp(b_2x)]^{-1},$$

where  $0 \leq b_1 < 1$  and  $0 \leq b_2 < 1$ . Three sets of parameters are tested:  $b_1 = 0.5$  and  $b_2 = 0$ ;  $b_1 = 0$  and  $b_2 = 0.25$ ; and  $b_1 = 0.5$  and  $b_2 = 0.25$ . The corresponding SSWs are denoted SSW1, SSW2, and SSW3, respectively. The steady state wave speeds of SSW1, SSW2, and SSW3 are  $c = 2.5$ ,  $c = 4.25$ , and  $c = 2.5$ , respectively. In the SSW3, the initial profile is given by the combination of two exponentials. Thus, as a general case, SSW3 is a good test problem for investigating the performance of the proposed asymptotic BC.

Taking  $N = 256$ ,  $\Delta x = 1.0$ , and  $\Delta t = 0.1$ , the proposed asymptotic BC is implemented in both the DSC and CN schemes, while the optimal suppression is employed in both the FPS and ASD methods. To simulate a long-term solution, the proposed moving frame method is utilized. The numerical solutions of Fisher's equation approximated by the four methods are shown in Table 4.6 and the simulated

TABLE 4.6

The errors of the wave solution speed ( $|c - \hat{c}|$ ) estimated by the DSC, CN, FPS ( $\epsilon = 2.0(-12)$ ), and ASD ( $\epsilon = 1.0(-11)$ ) schemes.

		$t = 100$	$t = 200$	$t = 300$	$t = 400$	$t = 500$
SSW1	DSC	1.76(-3)	9.49(-7)	5.68(-13)	2.84(-13)	0.0
	CN	4.75(-3)	8.72(-6)	6.49(-7)	1.42(-12)	8.52(-13)
	FPS	5.12(-1)	5.13(-1)	5.13(-1)	5.13(-1)	5.13(-1)
	ASD	5.94(-1)	5.86(-1)	5.88(-1)	5.88(-1)	5.88(-1)
SSW2	DSC	1.00(-8)	1.01(-8)	1.01(-8)	1.01(-8)	1.01(-8)
	CN	7.43(-9)	7.43(-9)	7.43(-9)	7.43(-9)	7.43(-9)
	FPS	2.26(+0)	2.26(+0)	2.26(+0)	2.26(+0)	2.26(+0)
	ASD	2.34(+0)	2.33(+0)	2.33(+0)	2.33(+0)	2.33(+0)
SSW3	DSC	1.56(-3)	8.77(-6)	8.52(-13)	2.84(-13)	0.0
	CN	5.78(-3)	9.59(-5)	9.94(-13)	2.84(-13)	2.84(-13)
	FPS	5.12(-1)	5.13(-1)	5.13(-1)	5.13(-1)	5.13(-1)
	ASD	5.94(-1)	5.86(-1)	5.87(-1)	5.88(-1)	5.88(-1)

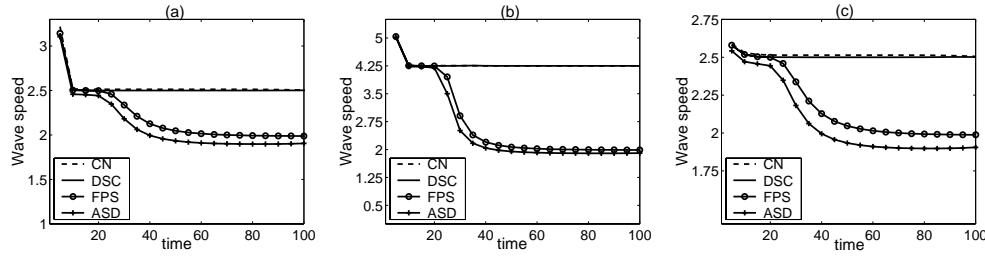


FIG. 4.6. The plots of the wave speed estimated by the four methods for SSWs. (a) SSW1; (b) SSW2; (c) SSW3.

wave speeds of the four methods are displayed in Figure 4.6. All numerical results are in excellent agreement with the theoretical analysis. The simulated wave speed of two spectral methods evolves gradually to the minimum speed  $c = 2$ , due to the suppression. The FPS results are relatively closer to theoretical value than those of the ASD method. By using the asymptotic BC, both the DSC and the CN generate similarly excellent results. When  $t < 300$ , the DSC results are more accurate than those of the CN method; when  $t > 300$ , the differences between the results of two schemes are negligible. Compared with the results obtained by the CN scheme for the strong reaction problem, the poor results obtained there are due to the low accuracy of the CN scheme. For the present case, the resolution of the CN scheme is sufficient to resolve the solutions. Thus, by using the asymptotic BC, excellent asymptotic solutions are obtained. In SSW3, amazingly accurate results are also achieved as in SSW1, which demonstrates the usefulness of the proposed simple asymptotic BC for the general applications. The only difference in the wave speeds of SSW1 and SSW3 is the starting wave speed; see Figure 4.6.

**5. Conclusion.** This paper explores the utility of the discrete singular convolution (DSC) algorithm for solving Fisher's equation. Several numerical issues that are crucial to the long-time behavior of the numerical solution of Fisher's equation are successfully treated in the present work. An accurate, robust, and efficient algorithm is constructed that yields sound simulation of the steady state of the equation. To further evaluate the present algorithm, three other standard methods are employed for a comparison. Fourier analysis is utilized to assess the spatial resolution of the four

methods. The temporal truncation orders of the four methods are clarified. Extensive numerical experiments are carried out to verify the theoretical analysis and to compare the accuracy, stability, flexibility, and efficiency of the four numerical schemes. Superspeed wave (SSW), which is numerically difficult, is chosen in the present study. All numerical results are validated either by analytical solutions or by the steady state wave speed.

Several interesting numerical issues of Fisher's equation are elaborated on in the present work. First, with strong reaction, the solution will evolve into a shock-like wave, which usually leads to inaccurate approximation. The numerical approximation could be greatly improved if a nonuniform moving mesh were used [16]. In the present study, it is demonstrated that, without utilizing a nonuniform mesh, the DSC and Fourier pseudospectral (FPS) schemes can produce much better results than those of [16]. This suggests that the high accuracy scheme could be a better way to resolve shock-like wave. Second, a moving frame method, which can automatically track the traveling wave, is introduced in the present work. This novel method provides an efficient and computationally feasible way to study long-time traveling wave solutions. Third, the SSW solution of Fisher's equation will quickly evolve into the minimum speed wave if an improper BC is applied at the right-hand boundary. Unfortunately, the only appropriate BC reported in the literature [8] requires a priori knowledge of the initial data, so it is not computationally applicable in general situations. To overcome this critical difficulty, a simple asymptotic scheme is proposed in the present work that is fully automatic and suitable for general applications. Numerical studies on three kinds of SSWs demonstrate the success of this new asymptotic scheme. Finally, with the new asymptotic scheme and moving frame method, the resulting DSC algorithm is shown to be an accurate, reliable, and efficient approach for solving Fisher's equation.

To further illustrate the performance of the DSC algorithm, three standard methods are employed to make a comparison for solving Fisher's equation. Based on this study, the following remarks can be made about these four methods:

1. The Fourier analysis indicates that the DSC scheme can provide spectral-like resolution over a broad range of wavenumbers. Comparable high accuracy is obtained in the numerical results of both the FPS and DSC schemes. The ASD scheme has limited accuracy because its temporal discretization is of  $O(\Delta t)$ , instead of  $O(\Delta t^5)$  as claimed in the original work [6].
2. The DSC is as flexible in handling complex geometries and BCs as the CN, whereas the two spectral methods are restricted to the periodic BC only. This inflexibility hinders the performance of two spectral methods for solving Fisher's equation because a correct numerical solution can only be achieved with appropriate BCs.
3. Undesirable oscillations are generated at the wave front in the numerical solutions approximated by the two spectral methods [6, 20, 2], and thus these solutions quickly become unstable. Such oscillations do not occur in the solutions of both the DSC and CN.
4. For a small number of grid points  $N$ , the DSC scheme usually requires more CPU time than the two spectral methods. However, when a large  $N$  is used in the strong reaction problem, the required CPU time of the FPS is longer than that of the DSC.

In summary, in terms of accuracy, flexibility, stability, and efficiency, the DSC algorithm performs well compared with other existing standard numerical methods for the solution of Fisher's equation.

## REFERENCES

- [1] J. CANOSA, *On a nonlinear diffusion equation describing population growth*, IBM J. Res. Develop., 17 (1973), pp. 307–313.
- [2] G. F. CAREY AND Y. SHEN, *Least-squares finite element approximation of Fisher's reaction-diffusion equation*, Numer. Methods Partial Differential Equations, 11 (1995), pp. 175–186.
- [3] R. A. FISHER, *The wave of advantage of advantageous genes*, Ann. Eugenics, 7 (1937), pp. 355–369.
- [4] B. FORNBERG, *On a Fourier method for the integration of hyperbolic equations*, SIAM J. Numer. Anal., 12 (1975), pp. 509–528.
- [5] B. FORNBERG, *The pseudospectral method: Comparisons with finite differences for the elastic wave equation*, Geophysics, 52 (1987), pp. 483–501.
- [6] J. GAZDAG AND J. CANOSA, *Numerical solution of Fisher's equation*, J. Appl. Probab., 11 (1974), pp. 445–457.
- [7] P. S. HAGAN, *Traveling wave and multiple traveling wave solutions of parabolic equations*, SIAM J. Math. Anal., 13 (1982), pp. 717–738.
- [8] T. HAGSTROM AND H. B. KELLER, *The numerical calculation of traveling wave solutions of nonlinear parabolic equations*, SIAM J. Sci. Stat. Comput., 7 (1986), pp. 978–988.
- [9] A. KOLMOGOROV, I. PETROVSHY, AND N. PISCOUNOFF, *Étude de l'équation de la diffusion avec croissance de la quantité de matière et son application à un problème biologique*, Bull. Univ. Etat Moscou Ser. Int. Sect. A Math. et Mecan., 1 (1937), pp. 1–25.
- [10] D. A. LARSON, *Transient bounds and time-asymptotic behavior of solutions to nonlinear equations of Fisher type*, SIAM J. Appl. Math., 34 (1978), pp. 93–103.
- [11] S. LI, L. R. PETZOLD, AND Y. REN, *Stability of moving mesh systems of partial differential equations*, SIAM J. Sci. Comput., 20 (1998), pp. 719–738.
- [12] T. MAVOUNGOU AND Y. CHERRUAULT, *Numerical study of Fisher's equation by Adomian's method*, Math. Comput. Modelling, 19 (1994), pp. 89–95.
- [13] R. E. MICKENS, *A best finite-difference scheme for the Fisher equation*, Numer. Methods Partial Differential Equations, 10 (1994), pp. 581–585.
- [14] R. E. MICKENS, *Relation between the time and space step-sizes in nonstandard finite-difference schemes for the Fisher equation*, Numer. Methods Partial Differential Equations, 13 (1997), pp. 51–55.
- [15] N. PAREKH AND S. PURI, *A new numerical scheme for the Fisher equation*, J. Phys. A, 23 (1990), pp. L1085–L1091.
- [16] Y. QIU AND D. M. SLOAN, *Numerical solution of Fisher's equation using a moving mesh method*, J. Comput. Phys., 146 (1998), pp. 726–746.
- [17] RIZWAN-UDDIN, *Comparison of the nodal integral method and nonstandard finite-difference schemes for the Fisher equation*, SIAM J. Sci. Comput., 22 (2001), pp. 1926–1942.
- [18] J. ROESSLER AND H. HÜSSNER, *Numerical solution of the (1+2)-dimensional Fisher's equation by finite elements and the Galerkin method*, Math. Comput. Modelling, 25 (1997), pp. 57–67.
- [19] B. F. SANDERS, N. K. KATOPODES, AND J. P. BOYD, *Spectral modeling of nonlinear dispersive waves*, J. Hydraulic Engrg., 124 (1998), pp. 2–12.
- [20] S. TANG AND R. O. WEBER, *Numerical study of Fisher's equation by a Petrov-Galerkin finite element method*, J. Austral. Math. Soc. Ser. B, 33 (1991), pp. 27–38.
- [21] R. VICHNEVETSKY AND J. B. BOWLES, *Fourier Analysis of Numerical Approximations of Hyperbolic Equations*, SIAM, Philadelphia, 1982.
- [22] Y. G. WANG, E. H. TWIZELL, AND W. G. PRICE, *Second-order, numerical methods for the solution of equations in population modelling*, Comm. Appl. Numer. Methods, 8 (1992), pp. 511–518.
- [23] G. W. WEI, *Quasi-wavelets and quasi interpolating wavelets*, Chem. Phys. Lett., 296 (1998), pp. 215–222.
- [24] G. W. WEI, *Discrete singular convolution for the solution of the Fokker-Planck equation*, J. Chem. Phys., 110 (1999), pp. 8930–8942.
- [25] G. W. WEI, *Solving quantum eigenvalue problems by discrete singular convolution*, J. Phys. B, 33 (2000), pp. 343–352.
- [26] G. W. WEI, *Discrete singular convolution for the sine-Gordon equation*, Phys. D, 137 (2000), pp. 247–259.
- [27] G. W. WEI, *A unified approach for the solution of the Fokker-Planck equation*, J. Phys. A, 33 (2000), pp. 4935–4953.
- [28] G. W. WEI, *Wavelets generated by using discrete singular convolution kernels*, J. Phys. A, 33 (2000), pp. 8577–8596.

- [29] G. W. WEI, *A new algorithm for solving some mechanical problems*, Comput. Methods Appl. Mech. Engrg., 190 (2001), pp. 2017–2030.
- [30] G. W. WEI, *Synchronization of single-side averaged coupling and its application to shock capturing*, Phys. Rev. Lett., 86 (2001), p. 3542–3546.
- [31] G. W. WEI, *Vibration analysis by discrete singular convolution*, J. Sound Vibration, 244 (2001), pp. 535–553.
- [32] G. W. WEI, *Discrete singular convolution for beam analysis*, Engrg. Structures, 23 (2001), pp. 1045–1053.
- [33] S. Y. YANG, Y. C. ZHOU, AND G. W. WEI, *Comparison of the discrete singular convolution algorithm and the Fourier pseudospectral method for solving partial differential equations*, Comput. Phys. Comm., 143 (2002), pp. 113–135.